Magnetic resonance imaging techniques for risk stratification in cardiovascular disease

Roes, S.D.

Chapter 9

Agreement and disagreement between contrast-enhanced magnetic resonance imaging and nuclear imaging for assessment of myocardial viability

S.D. Roes
T.A.M. Kaandorp
N. Ajmone Marsan
J.J.M. Westenberg
P. Dibbets-Schneider
M.P. Stokkel
H.J. Lamb
E.E. van der Wall
A. de Roos
J.J. Bax

Eur J Nucl Med Mol Imaging 2009;36:594-601

Abstract

Purpose

The purpose of this study was to compare contrast-enhanced magnetic resonance imaging (MRI) and nuclear imaging with ^{99m}Tc-tetrofosmin and ^{18}F- fluorodeoxyglucose (^{18}F-FDG) single photon emission computed tomography (SPECT) for assessment of myocardial viability.

Methods

Sixty patients with severe ischemic left ventricular (LV) dysfunction underwent contrast-enhanced MRI, ^{99m}Tc-tetrofosmin and ^{18}F-FDG SPECT. Myocardial segments were assigned a wall motion score from 0 (normokinesia) to 4 (dyskinesia) and a scar score from 0 (no scar) to 4 (76-100% transmural extent). Furthermore, ^{99m}Tc-tetrofosmin and ^{18}F-FDG segmental tracer uptake was categorized from 0 (tracer activity $>$ 75%) to 3 (tracer activity $<$ 25%). Dysfunctional segments were classified into viability patterns on SPECT: normal perfusion-^{18}F-FDG uptake, perfusion-^{18}F-FDG mismatch, and mild or severe perfusion-^{18}F-FDG match.

Results

Minimal scar was observed on contrast-enhanced MRI (scar score 0.4 $\pm$ 0.8) in segments with normal perfusion-^{18}F-FDG uptake, whereas extensive scar (scar score 3.1 $\pm$ 1.0) was noted in segments with severe perfusion-^{18}F-FDG match ($p < 0.001$). High agreement (91%) for viability assessment between contrast-enhanced MRI and nuclear imaging was observed in segments without scar tissue on contrast-enhanced MRI as well as in segment with transmural scar tissue (83%). Of interest, disagreement was observed in segments with subendocardial scar tissue on contrast-enhanced MRI.

Conclusion

Agreement between contrast-enhanced MRI and nuclear imaging for assessment of viability was high in segments without scar tissue and in segments with transmural scar tissue on contrast-enhanced MRI. However, evident disagreement was observed in segments with subendocardial scar tissue on contrast-enhanced MRI, illustrating that the non-enhanced epicardial rim can contain either normal or ischemically jeopardized myocardium.

Introduction

Assessment of viability is essential for optimization of treatment in patients with ischemic left ventricular (LV) dysfunction, since dysfunctional but viable myocardium is likely to improve after revascularization, whereas dysfunctional but nonviable myocardium will not benefit (1). Furthermore, patients with viable myocardium have better survival after revascularization than after medical treatment (2).

At the present time, several noninvasive imaging modalities are available for assessment of viability, including dobutamine echocardiography, single photon emission computed tomography (SPECT) and positron emission tomography (PET)(3-5). Nuclear imaging using tracers such as ^{99m}Tc-tetrofosmin and ^{18}F- fluorodeoxyglucose (^{18}F-FDG), allows evaluation of viability by assessment of myocardial perfusion and glucose utilization (4).

Contrast-enhanced magnetic resonance imaging (MRI) has been more recently introduced for assessment of viability (6-8). This technique offers visualization of scar tissue with high spatial resolution, enabling distinction between subendocardial and transmural scar (9). Kim et al. (6) reported that in segments without contrast-enhancement on MRI, recovery of function is highly likely to occur after revascularization, whereas improvement of function is unlikely in segments with extensive, transmural contrast-enhancement. However, difficulties arise in dysfunctional segments with subendocardial scar tissue, which show an intermediate extent of recovery, since contrast-enhanced MRI provides only information on scar tissue, whereas the non-enhanced (viable) tissue can contain either normal or ischemically jeopardized myocardium (10). Hence, the two imaging modalities discussed above provide different information on viability.

To our knowledge, only a few, relatively small studies evaluated patients with both contrast-enhanced MRI and nuclear imaging to determine viability (11-14). Consequently, the exact relationship between viability assessed with contrast-enhanced MRI and nuclear imaging is still largely unknown. Therefore, the purpose of the present study was to compare contrast-enhanced MRI and nuclear imaging with ^{99m}Tc-tetrofosmin and ^{18}F-FDG SPECT for assessment of viability in patients with severe ischemic LV dysfunction.

Methods

Study population

The study population consisted of 60 patients with severe ischemic LV dysfunction who underwent MRI, ^{99m}Tc-tetrofosmin SPECT and ^{18}F-FDG SPECT. Patients with myocardial infarction < 3 months before MRI or SPECT were excluded. Other exclusion criteria were (supra-) ventricular arrhythmias, pacemakers, intracranial clips and claustrophobia. Patient characteristics are listed in Table 1. The local ethics committee approved the study and all patients gave informed consent.

Table 1. Clinical characteristics of the study population.

Clinical variables	No. (%) of patients (n = 60)
Age (years)	65 ± 11
Men	50 (83)
Diabetes	16 (27)
Hypertension	14 (23)
Hypercholesterolemia	23 (38)
Smoking	25 (42)
Previous myocardial infarction	60 (100)
Prior revascularization	34 (57)
Percutaneous coronary intervention	20 (33)
Coronary artery bypass grafting	14 (23)
Extent of CAD (on coronary angiography)	
1-vessel disease	11 (18)
2-vessel disease	18 (30)
3-vessel disease	31 (52)
Medication	
β-Blockers	48 (82)
Calcium channel blockers	10 (17)
ACE inhibitors	55 (92)
Oral anticoagulants	59 (98)
Statins	48 (80)
Nitrates	28 (47)
Diuretics	56 (93)

ACE: angiotensin converting enzyme, CAD: coronary artery disease.

Magnetic resonance imaging: data acquisition

A 1.5T Gyroscan ACS-NT/Intera MRI scanner (Philips Medical Systems, Best, The Netherlands) equipped a 5-element cardiac synergy coil was used. Images were acquired during breath-holds of approximately 15 seconds using vector electrocardiographic gating.

The heart was imaged from apex to base (15) with 10-12 imaging levels (dependent on the heart size) in the short-axis view using a balanced turbo field echo sequence with parallel imaging (SENSE, acceleration factor 2). Typical parameters were a field of view of 400 × 320 mm^2, matrix of 256 × 206 pixels, slice thickness of 10.00 mm, no slice gap, flip angle of 35°, time to echo of 1.67 ms, and time to repeat of 3.3 ms. Temporal resolution was 25 to 39 ms. Geometric settings of baseline scans were stored and repeated for contrast-enhanced images to ensure matching of the same slices (and hence, myocardial segments).

Contrast-enhanced images were acquired approximately 15 minutes after bolus injection of gadolinium diethylenetriamine penta-acetic acid (Magnevist, Schering, Berlin, Germany; 0.15 mmol/kg) with an inversion-recovery 3D turbo field echo sequence; the inversion time was determined with a real-time plan scan. Typical parameters were a field of view of 400 × 300 mm^2, matrix of 256 × 192 pixels, slice thickness of 5.00 mm, flip angle of 15°, time to echo of 1.1 ms, and time to repeat of 3.00 ms.

Magnetic resonance imaging: data analysis

To determine global function, endocardial borders were outlined manually on short-axis cine images with previously validated software (MASS, Medis, Leiden, The Netherlands) (16). Papillary muscles were regarded as part of the ventricular cavity, and epicardial fat was excluded. LV end-systolic volume (ESV) and LV end-diastolic volume (EDV) were calculated. Subsequently, ESV was subtracted from EDV and LV ejection fraction (LVEF) was calculated.

To determine regional wall motion, cine MRI images were visually interpreted by 2 experienced observers using a 17-segment model (17). Each segment was assigned a wall motion/thickening score using a 5-point scale: 0: normal wall motion, 1: mild hypokinesia, 2: severe hypokinesia, 3: akinesia, and 4: dyskinesia. Wall thickening was taken into account for this classification, pre-empting the problem of postoperative paradoxical septal motion in patients with previous coronary artery bypass grafting.

Contrast-enhanced images were scored visually by 2 experienced observers using the 17-segment model described above (17). Segmental scarring was graded on each segment using the following 5-point scale: 0: absence of hyperenhancement, 1: hyperenhancement of 1% to 25% of LV wall thickness, 2: hyperenhancement extending from 26% to 50%, 3: hyperenhancement extending from 51% to 75%, and 4: hyperenhancement extending from 76% to 100%)(18).

^{99m}Tc-tetrofosmin SPECT: data acquisition

Imaging was performed at rest, with ^{99m}Tc-tetrofosmin (500 MBq) using a triple-head SPECT camera (GCA 9300/HG, Toshiba Corporation) equipped with low-energy, general-purpose collimators. A 20% window was used around the 140-keV energy peak of ^{99m}Tc-tetrofosmin. A total of 90 projections (step-and-shoot mode of 35 s/projection, total imaging time 23 min) were obtained over a 360° circular orbit. Data were stored in a 64 × 64, 16-bit matrix. The raw scintigraphic data were reconstructed with filtered back projection using a Butterworth filter (cut-off frequency 0.26 cycle per pixel, order 9). No attenuation correction was used.

^{99m}Tc-tetrofosmin SPECT: data analysis

Additional reconstruction yielded standard long- and short-axis projections perpendicular to the heart axis. Reconstructed slices were 6 mm in all directions. The short-axis slices were displayed in polar map format, adjusted for peak myocardial activity (100%). The myocardium was divided into 17 segments (17). Segmental tracer activity was categorized visually by 2 experienced observers on a 4-point scale: 0: normal tracer activity > 75%, 1: mildly reduced tracer activity 50%–75%, 2: moderately reduced tracer activity 25%–50%, and 3: severely reduced tracer activity < 25%.

^{18}F-FDG SPECT: data acquisition

^{18}F-FDG imaging, to evaluate myocardial glucose utilization, was performed on a separate day, after administration of acipimox (a nicotinic acid derivative, 500 mg, oral dose; Byk, Zwanenberg, The Netherlands) (19). Acipimox enhances myocardial ^{18}F-FDG uptake by reducing the plasma level of free fatty acids (20). After acipimox administration, the patients received a low-fat, carbohydrate-rich meal. This small meal further enhances myocardial ^{18}F-FDG uptake by stimulating endogenous insulin release (21). A blood sample was taken 60 minutes after acipimox administration to assess plasma glucose levels, and insulin was administered if needed. Then, 185 MBq ^{18}F-FDG was injected at rest. Data were acquired 45 minutes later at rest using the same SPECT system as described for perfusion imaging, with commercially available 511-KeV collimators. Data were acquired over 360° and stored in a 64 × 64, 16-bit matrix. From the raw scintigraphic data, transaxial slices were reconstructed by filtered back projection using a Butterworth filter (cut-off frequency 0.17 cycle per pixel, order 8). Attenuation correction was not applied.

^{18}F-FDG SPECT: Data analysis

Further reconstruction yielded standard short- and long-axis projections perpendicular to the heart axis. ^{18}F-FDG short-axis slides were displayed in polar map format, normalized to the maximum activity (set at 100%); the polar maps were divided into 17 segments (17). Segmental tracer activity was categorized visually by 2 experienced observers on a

4-point scale: 0: normal tracer activity > 75%, 1: mildly reduced tracer activity 50%–75%, 2: moderately reduced tracer activity 25%–50%, and 3: severely reduced tracer activity < 25%.

Definition of viability on nuclear imaging

The dysfunctional segments on cine MRI (wall motion score ≥ 1) were divided into four groups with different patterns of viability. Group 1 (normal perfusion-^{18}F-FDG uptake) consisted of segments with normal ^{99m}Tc-tetrofosmin activity (score 0) and normal ^{18}F-FDG activity (score 0). Group II (perfusion-^{18}F-FDG mismatch) consisted of segments with reduced ^{99m}Tc-tetrofosmin activity (score 1, 2 or 3) and preserved/ relatively increased ^{18}F-FDG activity (^{18}F-FDG score < ^{99m}Tc-tetrofosmin score). Group III (mild perfusion-^{18}F-FDG match) included segments with a mild reduction in ^{99m}Tc-tetrofosmin activity (score 1) and a concordant mild reduction in ^{18}F-FDG activity (score 1). Finally, group IV (severe perfusion-^{18}F-FDG match) consisted of segments with a moderate or severe reduction in ^{99m}Tc-tetrofosmin activity (score 2 or 3) and a concordant reduction in ^{18}F-FDG activity.

Statistical analysis

Continuous data were expressed as mean ± standard deviation (SD). One-way ANOVA analysis was used to compare scar score between the groups with different viability patterns. Comparison of proportions was performed using chi-square (χ^2) analysis. A p-value < 0.05 was considered statistically significant.

Results

Study Population

Clinical data are presented in Table 1. The mean age of the study population was 65 ± 11 years and 50 patients (83%) were men. All patients had evidence of coronary artery disease (CAD) on coronary angiography. No clinical events or interventions were reported between MRI and SPECT examinations.

Magnetic resonance imaging

Mean LVEF in the total study population was 27 ± 9%. The mean LV ESV and mean LV EDV were 250 ± 110 ml and 335 ± 114 ml, respectively.

A total of 1020 segments were analyzed, of which 692 (68%) showed abnormal wall motion. Of these dysfunctional segments, 91 (13%) showed mild hypokinesia, 248 (36%) showed severe hypokinesia, 298 (43%) segments were akinetic and 55 (8%) were dyskinetic.

Of the 692 dysfunctional segments, 484 (70%) revealed hyperenhancement, 105 (15%) showed minor hyperenhancement (scar score 1), 107 (15%) had a scar score of 2, 130 (19%) a scar score of 3, and 142 (21%) a scar score of 4.

^{99m}Tc-tetrofosmin SPECT

Of the 692 dysfunctional segments, 182 (26%) showed normal ^{99m}Tc-tetrofosmin activity (score 0). Ninety-one (13%) segments showed mildly reduced tracer activity (score 1), 147 (21%) showed moderately reduced tracer activity (score 2), and 272 (39%) showed severely reduced tracer activity (score 3).

^{18}F-FDG SPECT

Normal ^{18}F-FDG activity was observed in 220 (32%) segments of the 692 dysfunctional segments. Mildly reduced tracer activity (score 1) was seen in 157 (23%) segments, 108 (16%) segments showed moderately reduced tracer activity (score 2), and 207 (30%) segments showed severely reduced tracer activity (score 3).

Viability patterns assessed with nuclear imaging

Of the 692 dysfunctional segments, 183 (26%) showed normal perfusion-^{18}F-FDG uptake. A perfusion-^{18}F-FDG mismatch was observed in 145 (21%) segments. A mild perfusion-^{18}F-FDG match was seen in 73 (11%) segments and a severe perfusion-^{18}F-FDG match in 291 (42%) segments.

Of the 353 akinetic and dyskinetic segments, 40 (11%) segments showed normal perfusion-^{18}F-FDG uptake. In 78 (22%) segments, a perfusion-^{18}F-FDG mismatch was observed. A mild perfusion-^{18}F-FDG match and severe perfusion-^{18}F-FDG match were seen in respectively 35 (10%) and 200 (57%) segments.

Viability: nuclear imaging versus contrast-enhanced MRI

The mean scar score measured in the segments grouped according to viability pattern on nuclear imaging is presented in Figure 1. Minimal scar tissue was observed on contrast-enhanced MRI in segments with normal perfusion-^{18}F-FDG uptake on nuclear imaging (scar score 0.4 $\pm$ 0.8), whereas extensive scar tissue (scar score 3.1 $\pm$ 1.0) was noted in segments showing a severe perfusion-^{18}F-FDG match on nuclear imaging ($p < 0.001$).

Figure 1.

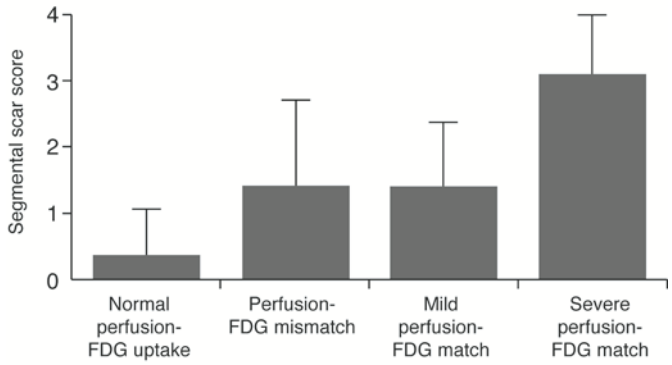

Mean scar score per segment assessed with contrast-enhanced MRI in segments grouped according viability pattern assessed with nuclear imaging (One-way ANOVA analysis: $p < 0.001$). Error bars represent standard deviation. FDG: ^{18}F- fluorodeoxyglucose.

Next (Figure 2), the dysfunctional segments were grouped according to the transmural extent of scar tissue on contrast-enhanced MRI. The majority of segments without scar on contrast-enhanced MRI (scar score 0, Figure 2A) showed normal perfusion-^{18}F-FDG uptake (67%) or a perfusion-^{18}F-FDG mismatch (24%). Considering viability, agreement in these segments was high (91%), since segments without scar on contrast-enhanced MRI as well as segments with normal perfusion-^{18}F-FDG uptake or a perfusion-^{18}F-FDG mismatch on nuclear imaging are regarded as viable tissue.

Figure 2.

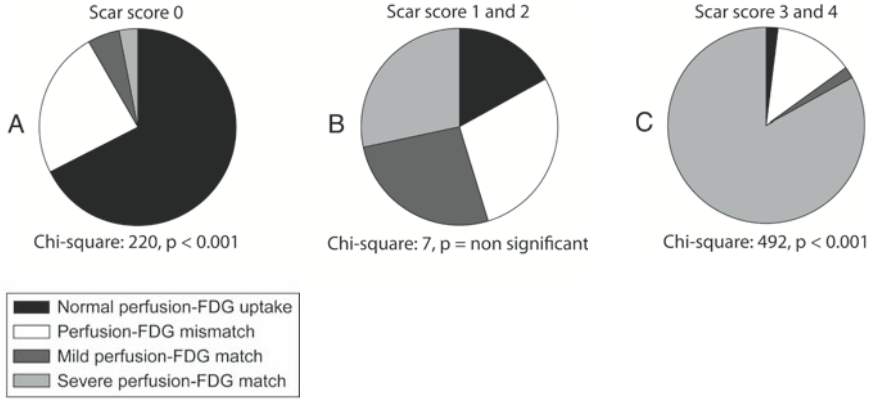

Relation between contrast-enhanced MRI and nuclear imaging for all dysfunctional segments showing the frequency of the four viability patterns assessed with nuclear imaging in segments without scar tissue (A), subendocardial scar tissue (B) and transmural scar tissue (C) on contrast-enhanced MRI. FDG: ^{18}F- fluorodeoxyglucose.

Conversely, the majority (83%) of segments with transmural scar on contrast-enhanced MRI (scar score 3 and 4, Figure 2C), showed a severe perfusion-^{18}F-FDG match on nuclear imaging. Accordingly, agreement in these segments was also high (83%), since segments with transmural scar on contrast-enhanced MRI and segments with a severe perfusion-^{18}F-FDG match on nuclear imaging represent non-viable tissue. Of note, in segments with subendocardial scar tissue on contrast-enhanced MRI (scar score 1 and 2, Figure 2B), the various viability patterns assessed with nuclear imaging were evenly distributed, indicating that segments with subendocardial scar on contrast-enhanced MRI, may have either normal perfusion-^{18}F-FDG uptake, perfusion-^{18}F-FDG mismatch, mild perfusion-^{18}F-FDG match or severe perfusion-^{18}F-FDG match. Figure 3 shows an example of a patient with subendocardial scar tissue on contrast-enhanced MRI and a perfusion-^{18}F-FDG mismatch on nuclear imaging.

Figure 3.

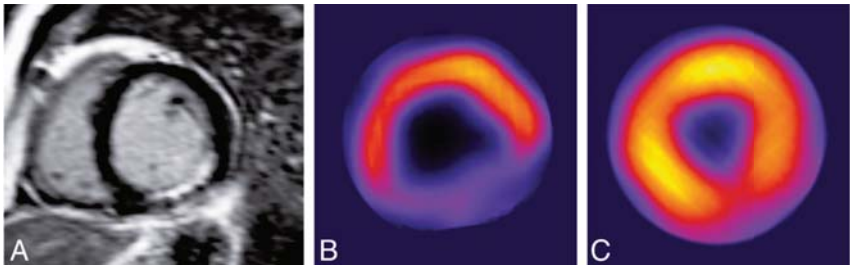

Example of a patient with inferior subendocardial scar tissue on contrast-enhanced MRI (A) and a severe reduction in ^{99m}Tc-tetrofosmin activity (B) but preserved ^{18}F-FDG activity (C) on SPECT (perfusion-^{18}F-FDG mismatch), indicating ischemically jeopardized myocardium, highlighting the discrepancy between information derived from contrast-enhanced MRI and nuclear imaging.

Finally (Figure 4), the akinetic and dyskinetic segments were analyzed separately. The majority of these segments without scar on contrast-enhanced MRI (scar score 0, Figure 4A), showed normal perfusion-^{18}F-FDG uptake (47%) or a perfusion-^{18}F-FDG mismatch (39%) on nuclear imaging. Consequently, agreement between the two techniques for assessment of viability was high (86%).

Conversely, in the majority of segments with transmural scar on contrast-enhanced MRI (scar score 3 and 4, Figure 4C), a severe perfusion-^{18}F-FDG match was observed on nuclear imaging (84%). Accordingly, agreement was also high (84%) in this category.

Of interest, in segments with subendocardial scar tissue on contrast-enhanced MRI (scar score 1 and 2, Figure 4B), the viability pattern on nuclear imaging varied highly between normal perfusion-^{18}F-FDG uptake, perfusion-^{18}F-FDG mismatch, mild perfusion-^{18}F-FDG match and severe perfusion-^{18}F-FDG match.

Figure 4.

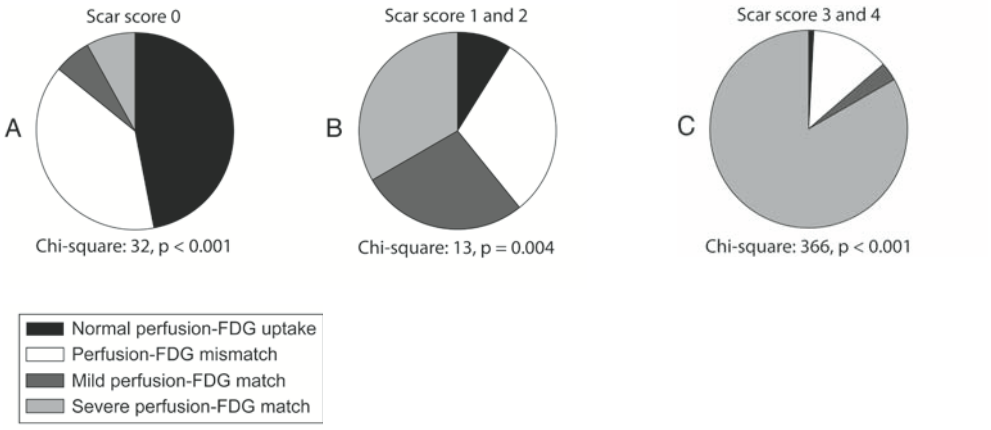

Relation between contrast-enhanced MRI and nuclear imaging for akinetic and dyskinetic segments showing the frequency of the four viability patterns assessed with nuclear imaging in segments without scar tissue (A), subendocardial scar tissue (B) and transmural scar tissue (C) on contrast-enhanced MRI. FDG: ^{18}F- fluorodeoxyglucose.

Discussion

The major finding in this study is that agreement between contrast-enhanced MRI and nuclear imaging for assessment of viability is high in segments without scar tissue as well as in segments with transmural scar tissue on contrast-enhanced MRI. Disagreement between the two imaging modalities regarding viability assessment is observed in segments with subendocardial scar tissue on contrast-enhanced MRI.

Contrast-enhanced MRI has been introduced as a reliable noninvasive technique for visualization of scar tissue in patients with previous myocardial infarction (6,18), and in patients with a clinical suspicion of CAD but without a history of myocardial infarction (22). Kim et al. (23) evaluated the accuracy of contrast-enhanced MRI for assessment of scar tissue in dogs with previous myocardial infarction and reported excellent agreement between the extent of scar tissue on contrast-enhanced MRI and the histological extent of necrosis.

Subsequently, Kim and colleagues (6) studied the value of scar tissue assessed with contrast-enhanced MRI for prediction of functional recovery after revascularization in 41 patients with chronic CAD. The authors reported that the majority of segments (78%) without scar tissue improved in function after revascularization, whereas improvement was virtually absent in segments with transmural scar tissue (6). Importantly, difficulties arise in segments with subendocardial scar tissue (transmural extent 1-50%), with only 53% of segments showing functional recovery (6).

Pooling of 4 studies in patients (n = 132) undergoing revascularization revealed high sensitivity (95%), but relatively low specificity (45%) of contrast-enhanced MRI to predict

improvement of function (10). The suboptimal specificity is related to segments with subendocardial scar tissue (transmural extent 1-50%) that do not improve in function. These findings highlight the fact that contrast-enhanced MRI is an excellent technique to delineate scar tissue (anatomical imaging), but the technique does not provide information on the pathophysiologic substrate of the non-scarred tissue, which results in suboptimal prediction of functional recovery after revascularization.

Combined perfusion-^{18}F -FDG imaging, as used in the current study, permits delineation of viability based on integration of perfusion and glucose utilization (24). This approach has been widely validated (both with PET and with SPECT imaging) for detection of viable myocardium and prediction of functional recovery (13,25,26). Different patterns of perfusion-^{18}F-FDG uptake can be observed. Dysfunctional but viable myocardium can be divided in normal perfusion and ^{18}F-FDG uptake representing repetitively stunned myocardium, whereas reduced perfusion with preserved ^{18}F-FDG uptake represents hibernation. Scar tissue can be divided (based on the concordant reduction in perfusion and ^{18}F-FDG uptake) into subendocardial scar tissue and transmural scar tissue. Based on these different patterns, with integration of perfusion and glucose utilization (assessed by ^{18}F-FDG imaging), it is possible to better characterize the substrate of the dysfunctional myocardium. Few studies have compared contrast-enhanced MRI with perfusion-^{18}F-FDG imaging (11-14,27). Kühl et al. (13) performed contrast-enhanced MRI and perfusion-^{18}F-FDG imaging in 29 patients with chronic CAD. Comparison between the techniques showed that viable segments on perfusion-^{18}F-FDG imaging contained minimal scar tissue, whereas the extent of scar tissue on contrast-enhanced MRI increased in parallel with the abnormalities on perfusion-^{18}F-FDG imaging; segments with severe matches on perfusion-^{18}F-FDG imaging showed transmural scar tissue on contrast-enhanced MRI (13).

Knuesel et al. (11) studied 19 patients with chronic CAD who underwent ^{13}N-ammonia PET to evaluate perfusion and ^{18}F-FDG PET to evaluate glucose utilization; scar tissue was analyzed with contrast-enhanced MRI. The authors reported a good correlation (ranging from $r = 0.62$ to $r = 0.82$) between segmental ^{18}F-FDG uptake and the transmurality of scar tissue on contrast-enhanced MRI. In particular, segments with ^{18}F-FDG uptake $\geq 50\%$ corresponded well with small areas of subendocardial scar tissue on contrast-enhanced MRI (and extensive non-scar tissue, 4.5 mm of the myocardial wall, on contrast-enhanced MRI). Ten patients also underwent revascularization, and the segments with preserved ^{18}F-FDG uptake and minimal scar tissue improved in function after revascularization; conversely, the segments with severely reduced ^{18}F-FDG uptake and extensive, transmural scar tissue, did not improve in function.

Of interest, the segments with severely reduced ^{18}F-FDG uptake, but non-transmural scar tissue on contrast-enhanced MRI, did not improve in function after revascularization. This is precisely the issue highlighted in the current study. The problem is that contrast-enhanced MRI provides excellent information on the extent and transmurality of scar tissue (better than any other imaging technique), but it does not provide information

on the pathophysiology of the non-scarred myocardium. As shown by Knuesel et al. (11), segments with small amount of scar tissue on contrast-enhanced MRI, but severely reduced ^{18}F-FDG uptake do not improve in function. These observations underscore the need to better characterize the non-scarred myocardium, as can be done with ^{18}F-FDG imaging (in combination with perfusion imaging). Indeed, the findings of the current study illustrate that segments with an intermediate transmurality of scar tissue (score 1 or 2) can exhibit a wide range of patterns on perfusion-^{18}F-FDG imaging (see Figure 2B).

An important limitation of the current study is the lack of outcome data after revascularization, which therefore does not provide information on the functional fate of the segments after revascularization (recovery or not). Additional studies in patients undergoing revascularization are needed to further explore the actual outcome of segments with intermediate amounts of scar tissue on contrast-enhanced MRI and different perfusion-^{18}F-FDG uptake patterns.

In conclusion, comparison of contrast-enhanced MRI and perfusion-^{18}F-FDG imaging for assessment of viability in patients with severe ischemic LV dysfunction revealed high agreement in segments without scar tissue on contrast-enhanced MRI as well as in segments with transmural scar tissue. However, evident disagreement was noted in segments with subendocardial scar tissue on contrast-enhanced MR, illustrating that the non-enhanced epicardial rim can contain either normal or ischemically jeopardized myocardium. This differentiation is potentially important for prediction of outcome after revascularization. Indeed, Bove et al. (28) demonstrated in 15 patients that further refinement of the non-scarred tissue (in this particular study assessment of contractile reserve by low-dose dobutamine challenge was used) resulted in superior prediction of outcome after revascularization. Further studies, comparing various imaging techniques in patients undergoing revascularization including information on segmental functional outcome are needed to better define the contribution of scar tissue and viable tissue to functional recovery after revascularization.

References

1. Rahimtoola SH. The hibernating myocardium. Am Heart J 1989;117:211-221.
2. Allman KC, Shaw LJ, Hachamovitch R, et al. Myocardial viability testing and impact of revascularization on prognosis in patients with coronary artery disease and left ventricular dysfunction: a meta-analysis. J Am Coll Cardiol 2002;39:1151-1158.
3. Bax JJ, Cornel JH, Visser FC, et al. Prediction of recovery of myocardial dysfunction after revascularization. Comparison of fluorine-18 fluorodeoxyglucose/thallium-201 SPECT, thallium-201 stress-reinjection SPECT and dobutamine echocardiography. J Am Coll Cardiol 1996;28:558-564.
4. Bax JJ, van der Wall EE, Harbinson M. Radionuclide techniques for the assessment of myocardial viability and hibernation. Heart 2004;90 Suppl 5:v26-v33.
5. Cornel JH, Bax JJ, Fioretti PM. Assessment of myocardial viability by dobutamine stress echocardiography. Curr Opin Cardiol 1996;11:621-626.
6. Kim RJ, Wu E, Rafael A, et al. The use of contrast-enhanced magnetic resonance imaging to identify reversible myocardial dysfunction. N Engl J Med 2000;343:1445-1453.
7. Isbell DC, Kramer CM. Cardiovascular magnetic resonance: structure, function, perfusion, and viability. J Nucl Cardiol 2005;12:324-336.
8. Isbell DC, Kramer CM. Magnetic resonance for the assessment of myocardial viability. Curr Opin Cardiol 2006;21:469-472.
9. Lee VS, Resnick D, Tiu SS, et al. MR imaging evaluation of myocardial viability in the setting of equivocal SPECT results with (99m)Tc sestamibi. Radiology 2004;30:191-197.
10. Kaandorp TA, Lamb HJ, van der Wall EE, et al. Cardiovascular MR to access myocardial viability in chronic ischaemic LV dysfunction. Heart 2005;91:1359-1365.
11. Knuesel PR, Nanz D, Wyss C, et al. Characterization of dysfunctional myocardium by positron emission tomography and magnetic resonance: relation to functional outcome after revascularization. Circulation 2003;108:1095-1100.
12. Kuhl HP, Beek AM, van der Weerdt AP, et al. Myocardial viability in chronic ischemic heart disease: comparison of contrast-enhanced magnetic resonance imaging with (18)F-fluorodeoxyglucose positron emission tomography. J Am Coll Cardiol 2003;41:1341-1348.
13. Kuhl HP, Lipke CS, Krombach GA, et al. Assessment of reversible myocardial dysfunction in chronic ischaemic heart disease: comparison of contrast-enhanced cardiovascular magnetic resonance and a combined positron emission tomography-single photon emission computed tomography imaging protocol. Eur Heart J 2006;27:846-853.
14. Wu YW, Tadamura E, Yamamuro M, et al. Comparison of contrast-enhanced MRI with (18)F-FDG PET/201Tl SPECT in dysfunctional myocardium: relation to early functional outcome after surgical revascularization in chronic ischemic heart disease. J Nucl Med 2007;48:1096-1103.
15. Lamb HJ, Doornbos J, van der Velde EA, et al. Echo planar MRI of the heart on a standard system: validation of measurements of left ventricular function and mass. J Comput Assist Tomogr 1996;20:942-949.

16. van der Geest RJ, Buller VG, Jansen E, et al. Comparison between manual and semiautomated analysis of left ventricular volume parameters from short-axis MR images. J Comput Assist Tomogr 1997;21:756-765.
17. Cerqueira MD, Weissman NJ, Dilsizian V, et al. Standardized myocardial segmentation and nomenclature for tomographic imaging of the heart: a statement for healthcare professionals from the Cardiac Imaging Committee of the Council on Clinical Cardiology of the American Heart Association. Circulation 2002;105:539-542.
18. Wu E, Judd RM, Vargas JD, et al. Visualisation of presence, location, and transmural extent of healed Q-wave and non-Q-wave myocardial infarction. Lancet 2001;357:21-28.
19. Schinkel AF, Bax JJ, Valkema R, et al. Effect of diabetes mellitus on myocardial 18F-FDG SPECT using acipimox for the assessment of myocardial viability. J Nucl Med 2003;44:877-883.
20. Nuutila P, Knuuti MJ, Raitakari M, et al. Effect of antilipolysis on heart and skeletal muscle glucose uptake in overnight fasted humans. Am J Physiol 1994;267:E941-E946.
21. Bax JJ, Veening MA, Visser FC, et al. Optimal metabolic conditions during fluorine-18 fluorodeoxyglucose imaging; a comparative study using different protocols. Eur J Nucl Med 1997;24:35-41.
22. Kwong RY, Chan AK, Brown KA, et al. Impact of unrecognized myocardial scar detected by cardiac magnetic resonance imaging on event-free survival in patients presenting with signs or symptoms of coronary artery disease. Circulation 2006;113:2733-2743.
23. Kim RJ, Fieno DS, Parrish TB, et al. Relationship of MRI delayed contrast enhancement to irreversible injury, infarct age, and contractile function. Circulation 1999;100:1992-2002.
24. Bax JJ, Visser FC, Elhendy A, et al. Prediction of improvement of regional left ventricular function after revascularization using different perfusion-metabolism criteria. J Nucl Med 1999;40:1866-1873.
25. Bax JJ, Cornel JH, Visser FC, et al. Prediction of improvement of contractile function in patients with ischemic ventricular dysfunction after revascularization by fluorine-18 fluorodeoxyglucose single-photon emission computed tomography. J Am Coll Cardiol 1997;30:377-383.
26. Bax JJ, Patton JA, Poldermans D, et al. 18-Fluorodeoxyglucose imaging with positron emission tomography and single photon emission computed tomography: cardiac applications. Semin Nucl Med 2000;30:281-298.
27. Klein C, Nekolla SG, Bengel FM, et al. Assessment of myocardial viability with contrast-enhanced magnetic resonance imaging: comparison with positron emission tomography. Circulation 2002;105:162-167.
28. Bove CM, Dimaria JM, Voros S, et al. Dobutamine response and myocardial infarct transmurality: functional improvement after coronary artery bypass grafting-initial experience. Radiology 2006;240:835-841.